Chemical Engineering Journal 487 (2024) 150412

Contents lists available at ScienceDirect

Chemical Engineering Journal

journal homepage: www.elsevier.com/locate/cej

Boosted outputs and robustness of polymeric tribovoltaic nanogenerator through secondary doping

Jia Meng [a,b], Chuntao Lan [a], Chongxiang Pan [a,b], Jun Yang [a,b], Xiong Pu [a,b,c,*], Zhong Lin Wang [a,c,d,e,f,*]

[a] CAS Center for Excellence in Nanoscience, Beijing Key Laboratory of Micro-nano Energy and Sensor, Beijing Institute of Nanoenergy and Nanosystems, Chinese Academy of Sciences, Beijing 101400, China
[b] Center on Nanoenergy Research, Institute of Science and Technology for Carbon Peak & Neutrality, Key Laboratory of Blue Energy and Systems Integration (Guangxi University), Education Department of Guangxi Zhuang Autonomous Region, School of Physical Science & Technology, Guangxi University, Nanning 530004, China
[c] School of Nanoscience and Engineering, University of Chinese Academy of Sciences, Beijing 100049, China
[d] School of Materials Science and Engineering, Georgia Institute of Technology, Atlanta, Georgia 30332-0245, USA
[e] Guangzhou Institute of Blue Energy, Knowledge City, Huangpu District, Guangzhou 510555, China
[f] Yonsei Frontier Lab, Yonsei University, Seoul 03722, Republic of Korea

ARTICLE INFO

Keywords:
Tribovoltaic nanogenerator
Energy band engineering
Metal-semiconductor interface
Polymer semiconductor
Triboelectric nanogenerator

ABSTRACT

The semiconductor-based tribovoltaic nanogenerator (TVNG) garners distinctive characteristics of direct current output at low internal impedance, rendering it great potentials for self-powered electronics. We present a polymeric TVNG for achieving enhanced electrical outputs and robustness through secondary doping strategy. By utilizing the dimethyl sulfoxide (DMSO) as a dopant, the transport properties of semiconducting poly(3,4-ethylenedioxythiophene):poly(styrene sulfonate) (PEDOT:PSS) can be modulated. We then demonstrate that the tribovoltaic outputs can be significantly enhanced due to the improved conductivity of the PEDOT:PSS and the enlarged Schottky barrier at the dynamic metal–semiconductor interfaces. The quantity of the transferred charge per motion cycle can reach 150.48 mC m^{-2} in contact-separation mode and 225.73 mC m^{-2} in sliding mode. Meantime, the dopant improves the flexibility of the PEDOT:PSS and hence the mechanical robustness of TVNG, allowing stable outputs for ~ 100,000 contact-separation operations cycles or ~ 36,000 bending cycles. Furthermore, the device also demonstrates exceptional humidity resistance, but confirms a coupling of tribovoltaic effect and electrochemical effect in high-humidity conditions (relative humidity over 90%). Therefore, our findings provide insightful strategies for future optimization of practical tribovoltaic devices.

1. Introduction

The advancement of the internet of things has precipitated an increasing demand for sustainable and distributed energy sources [1]. Batteries and supercapacitors are currently applied as the major power sources, but they need to be recharged frequently and their recycling or post-processing is accompanied with environmental issues [2]. Self-powering devices [3], such as solar cells [4], triboelectric nanogenerators [5], piezoelectric nanogenerators [6], etc, which convert energy from surrounding environment into electricity [7], will be excellent alternative candidates for energy supply [8,9]. Among them, a novel type of semiconductor direct-current generator based on tribovoltaic effect [10,11] has been widely investigated owing to its simple structure [12], low internal resistance [13] and high current density [14]. The tribovoltaic nanogenerators (TVNG) is characterized by the mechano-electrical energy conversion at dynamic semiconductor interfaces, mainly including metal–semiconductor [15], semiconductor–semiconductor [16], semiconductor-insulator-semiconductor [17], and liquid-semiconductor dynamic interfaces [18]. This structure diversity of TVNG makes it suitable for harvesting mechanical energy in a variety of scenarios [19] and applicable for powering small electronic devices [20]. Nevertheless, high electrical outputs and excellent durability of TVNG are urgently demanded for practical applications.

The electrical outputs of the TVNG are intrinsically related to the energy band structures of the dynamic interfaces. Specifically, the output voltage can be tuned by the Fermi energy level difference [21] or

* Corresponding authors.
E-mail addresses: puxiong@binn.cas.cn (X. Pu), zhong.wang@mse.gatech.edu (Z. Lin Wang).

https://doi.org/10.1016/j.cej.2024.150412
Received 3 January 2024; Received in revised form 22 February 2024; Accepted 13 March 2024
Available online 14 March 2024

the interface junction barrier height [22]. Several studies show that the increased barrier height is beneficial for the higher voltage [23], as it is the internal built-in electric field that separates the mechanically excited electron-hole pairs. Therefore, the outputs of TVNG can be modulated by selecting appropriate materials to form dynamic metal–semiconductor or semiconductor–semiconductor interfaces. To further enhance the separation of excited charge carriers, extra interface polarization field, like ferroelectric polarization field, has been introduced [24]. Very recent works show that the interface electrostatic field existing in some wide-bandgap semiconductors (like GaN) can even significantly boost the voltage outputs [25,26]. As for the robustness of the TVNG, the mechanical abrasion is a big challenge for the practical applications [27]. Meantime, most high-quality semiconductors are too rigid or brittle to withstand large deformation possibly encountered in practical

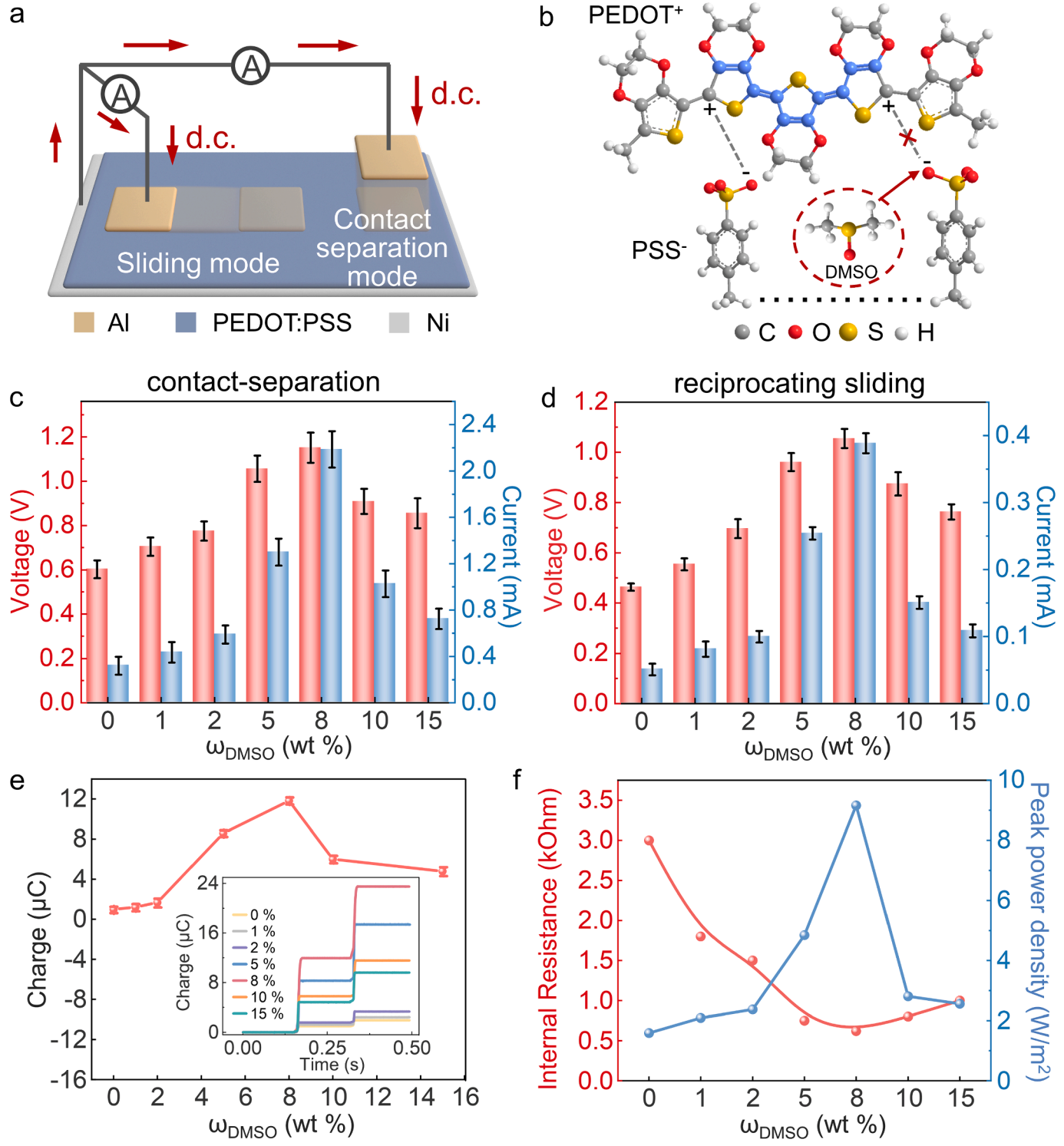

Fig. 1. The effect of doping on the outputs of tribovoltaic nanogenerator (TVNG). (a) Schematic illustration of the TVNG working in either sliding or contact-separation mode. (b) Schematic illustration of the doping mechanism. Variation of the electrical outputs of TVNG with the DMSO weight percentages in (c) contact-separation and (d) sliding mode. Variation of (e) transferred charge quantity per motion cycle, and (f) matched power and impedance with the doping content, respectively.

devices [28]. Therefore, polymer semiconductors [29,30] or perovskite materials [31] are used as the semiconductor friction layer to improve the flexibility and durability. Strategies like interface lubricants [32] or replacing sliding friction with rolling friction [33] were demonstrated to alleviate mechanical wear. Furthermore, it is also demonstrated that the TVNG working at contact-separation mode can decouple the mechanical wear effect and tribovoltaic effect, so as to avoid the mechanical abrasion [34]. Despite these progresses, further efforts are still required to improve the outputs and durability of the TVNGs.

In this work, we present a polymeric tribovoltaic nanogenerator based on Al/PEDOT:PSS dynamic interface with improved electrical outputs and enhanced robustness via secondary doping. The doping reagent DMSO was employed to modulate the transport properties of the PEDOT:PSS film, and the electrical outputs of the TVNG. It is found that, at an optimum DMSO content of 8 wt%, the TVNG reached a peak short-circuit current density of 27.85 A/m^{-2} and 4.97 A/m^{-2} in contact-separation mode and sliding mode, respectively. The peak power density reached 9.16 W m^{-2} at a matched impedance of about 620 Ohm in contact-separation mode. Systematic characterizations were investigated to demonstrate that the enhanced electrical outputs are attributed to the improved electrical properties of the polymer semiconductor PEDOT:PSS film and the optimized Al/PEDOT:PSS junction characteristics. Furthermore, the secondary doping was proven to enhance the flexibility of the PEDOT:PSS film, and thus the mechanical robustness of the TVNG. Besides, the device exhibited excellent humidity resistance, but confirmed a coupling of tribovoltaic effect and electrochemical effect at very high humidity environment (relative humidity over 90%). Therefore, our studies present an effective approach to enhance both the electrical outputs and robustness of the practically viable tribovoltaic devices.

2. Results and discussion

2.1. Electricity generation characteristics

To achieve high output performances of tribovoltaic devices, it is of great significance to regulate the band structures and transport properties of the semiconductor layer. In this context, a TVNG with a dynamic Schottky interface between metallic Al and PEDOT:PSS was designed, where the secondary doping of PEDOT:PSS was conducted to modulate its electrical properties. Briefly, the TVNG consists of three parts, the bottom electrode Ni tape, the polymer semiconductor PEDOT:PSS film, and an Al electrode that slides or contacts-separates with PEDOT:PSS film. As depicted in Fig. 1a, the generator working at both the sliding and contact-separation modes can generate DC electrical outputs. In this work, dimethyl sulfoxide (DMSO), a common high-boiling point solvent, was utilized as a secondary doping reagent to regulate the band structures and transport properties of PEDOT:PSS. The doping mechanism is that the Coulombic interaction between PEDOT and PSS is reduced by a shielding effect of the polar solvents, which induces conformational change in PEDOT chains and thereby enhances the conductivity of the PEDOT:PSS film (Fig. 1b). The films with different conductivities were obtained by using a series of doping weight percentages. The preparation process of the doped PEDOT:PSS thin films is detailed in Figure S1 where the weight content of DMSO (ω_{DMSO}) varied from 0% to 15%. As shown in Fig. 1c and 1d, the open-circuit voltage and short-circuit current of TVNG firstly boosted with increasing ω_{DMSO} from 0% to 8% and then reduced as further increasing ω_{DMSO} from 8% to 15%, both in contact-separation and sliding modes. The maximum output of TVNG achieved at ω_{DMSO} of 8%, with a peak voltage of 1.15 V and a peak current of 2.18 mA (27.85 A/m^{-2}) in contact separation mode (see also the output profiles in Figure S2), and a peak voltage of 1.05 V and a peak current of 0.39 mA (4.97 A/m^{-2}) in sliding mode (see profiles in Figure S3). The transferred charge per motion cycle of the DC generator also reached a maximum of 11.82 μC (150.48 mC m^{-2}) in contact separation mode and 17.72 μC (225.73 mC m^{-2}) in the sliding mode (Fig. 1e and Figure S4). Furthermore, when increasing ω_{DMSO}, the internal impedance of the generators in contact-separation mode decreased firstly from 3.0 kOhm to 0.62 kOhm and then slightly increased to 1.0 kOhm (Fig. 1f). The peak power of TVNG, showing the opposite trend, reached maximum of 9.16 W m^{-2} at 8% of ω_{DMSO} (Figure S5), which is 5.76 times higher than the value of the TVNG without secondary doping treatment.

2.2. Electrical and mechanical properties of doped PEDOT:PSS films

In order to understand the effect of the dopant DMSO on the outputs of TVNGs, the variation of the materials properties of PEDOT:PSS films were studied at first. As depicted in Fig. 2a, the electrical conductivity, charge mobility, and carrier concentration of the PEDOT:PSS films increased with DMSO content at first (ω_{DMSO} from 0% to 8%) and then decreased gradually (ω_{DMSO} from 8% to 15%). Noteworthy, even when ω_{DMSO} reached 15%, the electrical conductivity, charge mobility and carrier concentration are still higher than those of pristine PEDOT:PSS film. In PEDOT:PSS, hydrophobic, conductive PEDOT-rich grains are embedded in a hydrophilic, insulating PSS-rich matrix [35], and the PSS$^-$ acts as a soluble charge-balancing counterion of PEDOT$^+$. The increased conductivity is attributed to the dopant-induced conformational changes in the PEDOT chains. As the dopants reduce the interaction between PEDOT and PSS, the self-assembly of PEDOT chains will be improved and the π-π stacking can be enhanced. When the PEDOT configuration changes from a coil to a more linear crystalline structure [36], the resistance for the inter-lamella hopping of carriers is reduced [37]. Meantime, the PEDOT grain size can be increased, and the π-π stacking distance within the grains can be reduced [38]. Therefore, the enhanced π-π stacking improves the charge transfer between PEDOT chains. The XRD patterns of PEDOT:PSS samples treated with ω_{DMSO} ranging from 0% to 15% were displayed in Fig. 2b. The characteristic peak of doped PEDOT:PSS is located at ~ 26.4°, corresponding to the lattice spacing of approximately 3.37 Å, which is slightly smaller than that of the initial value of 3.53 Å (25.2°). Therefore, it is confirmed that the DMSO dopants reduced π-π stacking distance [$d_{(0\,1\,0)}$] of the aromatic rings of PEDOT (as schemed in Figure S6). Furthermore, the improved crystallinity by the dopants can be inferred from the stronger and sharper diffraction peaks (Fig. 2b). Therefore, this effect of the dopants on the transport properties are summarized in Fig. 2c, where the enhanced PEDOT π-π stacking and improved crystallinity account for the promoted charge transfer mobility. The enhanced carrier concentration originates from the conversion of more thiophene rings in PEDOT from benzoic acid to quinoid-type compounds [39], which is evidenced by the red-shift phenomenon in the FTIR spectrum (Figure S7). This process creates more positive charges (holes) within the thiophene ring, evidenced by a blue shift of all bands in the Raman spectrum (Figure S8). However, at an excessive DMSO doping content, phase separation occurs to form a nonuniform PEDOT:PSS film (Figure S9). The PEDOT chains are completely surrounded by DMSO, which in turn acts as a scattering center [40], so that backscattering is increased and carrier mobility is decreased [41].

Furthermore, DMSO doping endows the PEDOT:PSS film with enhanced mechanical properties, which is essential for achieving better flexibility and robustness of TVNG device. DMSO acts as a plasticizer, which aids in reorientation of PEDOT/PSS chains under deformations. As demonstrated in Fig. 2d and Figure S10, the elongation at break of the PEDOT:PSS film increased from 3.69% to 27.44% with ω_{DMSO} increased from 0% to 8%, but subsequently decreased as ω_{DMSO} is increased further. The tensile strength shows the similar trend, but the Young's modulus decreased gradually with increased DMSO content, which results in the reduced film rigidity and increased ductility. At 8% DMSO doping content, the elongation at break is increased by ~ 7 times, the tensile strength is increased by ~ 2 times, and the Young's modulus is reduced to ~ 40% of the pristine value. The photos and micromorphology of the doped PEDOT:PSS film (ω_{DMSO} of 8%) at different

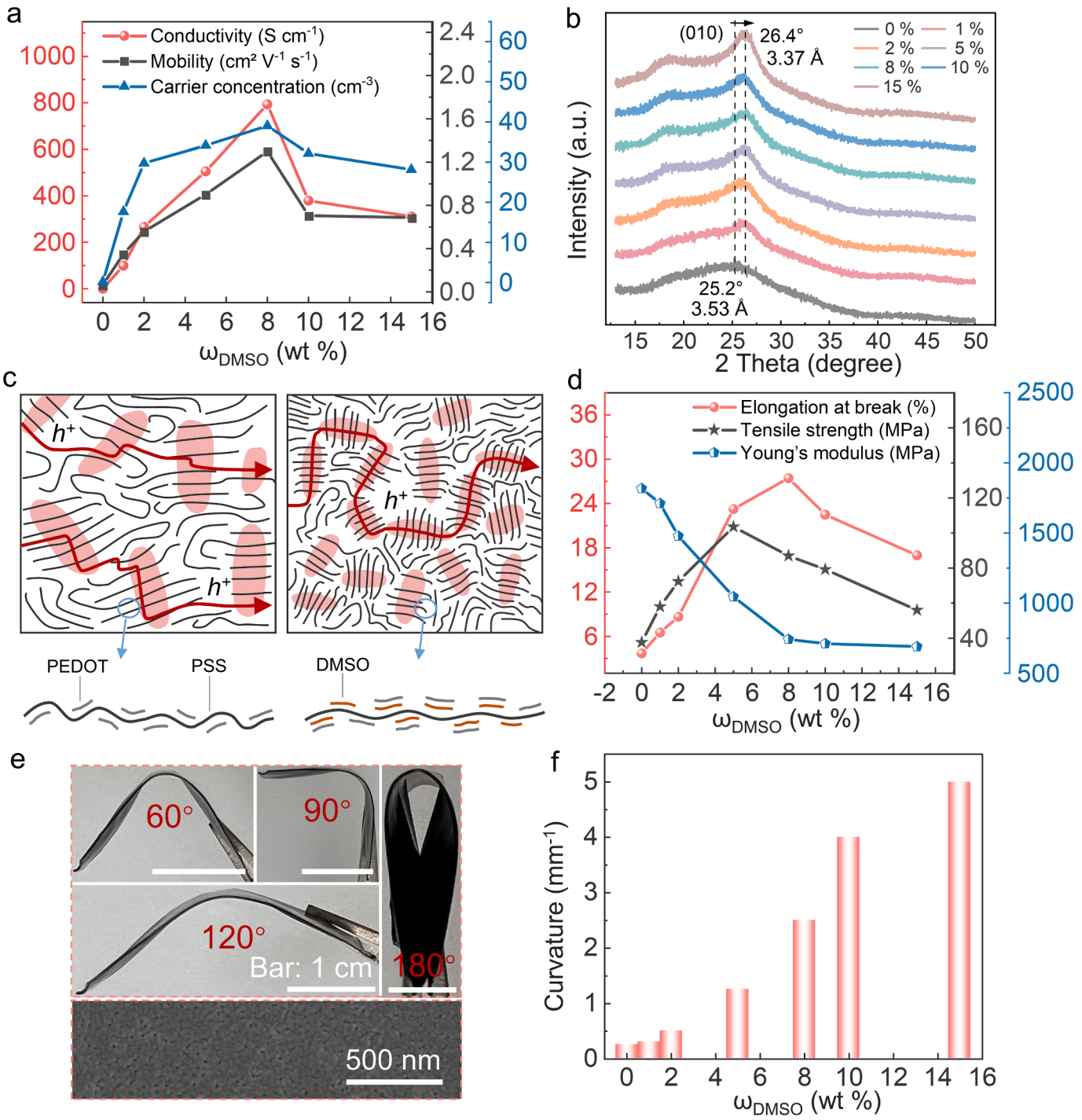

Fig. 2. The effect of doping on the electrical and mechanical properties of PEDOT:PSS films. (a) Conductivity, mobility, and carrier concentration of pristine and doped PEDOT:PSS. (b) X-ray diffraction patterns measured from PEDOT:PSS samples. (c) Schematic illustration of the charge transport of pristine and DMSO-doped PEDOT:PSS films. (d) The variation of mechanical properties with the dopant weight percentages. (e) Photos of PEDOT:PSS films doped with 8 wt% DMSO. (f) variation of the maximum curvature of PEDOT:SS thin films with dopant weight percentages.

bending angles indicate excellent flexibility of the film (Fig. 2e). The maximum curvature of the PEDOT:PSS film gradually increased with ω_{DMSO} from 0% to 15%, further indicating the enhanced softness and flexibility (Fig. 2f). Other similar polar solvents [42] or ionic liquids [43] are also good candidates as secondary dopants, allowing flexible tuning of the molecular structure, electrical and mechanical properties of PEDOT:PSS polymer.

2.3. The effects of dopants on junction characteristics and tribovoltaic outputs

The output performances of a TVNG device with dynamic metal–semiconductor interface are related to the metal–semiconductor Fermi level difference and the impedance of the entire device, both of which are largely dependent on the energy band structure of the semiconductor. In Figure S11, the UPS spectra of pristine and doped PEDOT:PSS films are presented, accompanied by detailed high and low binding

energy cutoffs in Figure S12. According to the UV–Vis diffuse reflectance spectra of the pristine and the doped PEDOT:PSS films, the optical bandgap of PEDOT:PSS films changed slightly ranging from 1.7 eV to 1.6 eV (Figure S13). The band structure of doped PEDOT:PSS films were calculated by combining the measurement results of these two spectra, as detailed in Supplementary Note 3. The energy band structures of the doped PEDOT:PSS films and metal Al are then depicted in Fig. 3a. It can be suggested that all these samples can form Schottky contacts with the Al electrode, and the junction barrier height should be the maximum when the doping content is 8%. This measured band structure is consistent with experiment *I-V* curves (Fig. 3b). The *I-V* curves of all the metal–semiconductor junctions exhibit the rectification phenomenon

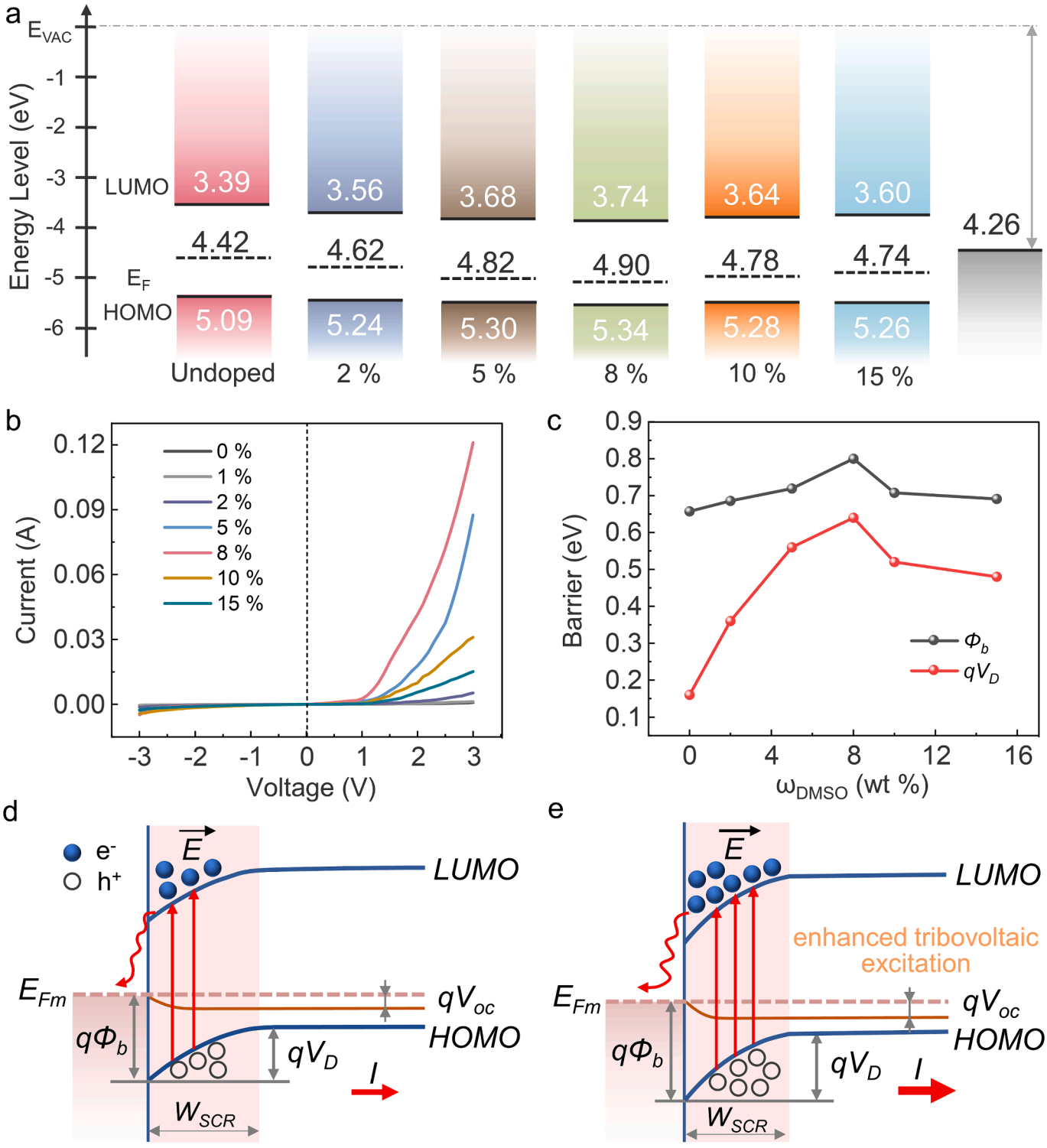

Fig. 3. The energy band structure and tribovoltaic effect at Al and PEDOT:PSS interfaces. (a) Energy level diagram of PEDOT:PSS doped with different weight percentages of DMSO based on parameters obtained from UPS spectra and UV–Vis diffuse reflectance spectra. (b) The current–voltage curves of the Al-PEDOT:PSS junction with different dopant percentages. (c) The Schottky barrier heights calculated from *I to V* curves and Fermi level differences calculated from energy band structure. Energy band diagrams showing the comparison of the tribovoltaic effect using (d) pristine and (e) doped PEDOT:PSS.

and the Schottky junction characteristics. The rectification ratios of Schottky junctions were calculated and presented in Table S1. Evidently, when ω_{DMSO} is 8%, the rectification ratio of Al-PEDOT reaches the maximum at 25.27. According to the thermionic emission theory, the barrier height (Φ_b) of the Schottky device can be calculated:

$$I = I_S \exp\left(\frac{qV}{nkT}\right) \quad (1)$$

$$I_S = AA^*T^2 \exp\left(-\frac{q\phi_b}{kT}\right) \quad (2)$$

$$InI = InI_S + \frac{qV}{nkT} \quad (3)$$

$$\phi_b = \frac{kT}{q} \ln\left(\frac{AA^*T^2}{I_S}\right) \quad (4)$$

where A^* is the effective Richardson constant (equal to 120 A cm^{-2} K^{-2} for free electrons), k is the Boltzmann constant (8.62×10^{-5} eV K^{-1}), e is electronic charge, T is absolute temperature, A is the junction contact area, I_S is the saturation current, n is ideality factor, and V is the bias voltage. The experimental data is plotted as ln I vs. V, and Φ_b and n is calculated from intercept and slope of the linear fit to the linear part of forward characteristics. The calculated Schottky barrier heights (Φ_b) are 0.657 eV, 0.685 eV, 0.719 eV, 0.800 eV, 0.708 eV and 0.690 eV, as ω_{DMSO} ranging from 0% to 15% (Fig. 3c). The barrier height is increased with increasing ω_{DMSO} from 0% to 8%, and is decreased as further increasing ω_{DMSO} from 8% to 15%. This variation trend of the junction barrier height is consistent with that calculated from the optical spectra.

Therefore, the effects of the dopants on the tribovoltaic outputs can be inferred based on the variation trends of the semiconductor properties and the junction characteristics. The energy band diagram of the metal–semiconductor interfaces of undoped PEDOT:PSS film and doped PEDOT:PSS film are presented in Fig. 3d and Fig. 3e, respectively. In the initial device (Fig. 3d), the Fermi level difference is 0.16 eV and the Schottky barrier height is 0.657 eV. In the energy band diagram of the device composed of doped film (ω_{DMSO} of 8%), the Schottky barrier is increased to 0.80 eV and the Fermi level difference is increased to 0.64 eV. According to the tribovoltaic effect, nonequilibrium electron-hole pairs are excited in the charge-depletion area by the mechanical energy either in sliding motion mode or contact-separation mode. The internal electric field in the junction will separate the excited electron-hole pairs to generate current in external circuit. Therefore, higher junction barrier and stronger internal fields are helpful to effectively separate excited charge carriers, contributing to a higher current. Simultaneously, the Fermi level of PEDOT:PSS drops more toward the lower energy level of the HOMO (expanded qV_{OC}), resulting in elevated potential in the external circuit. In addition, the surface states of the PEDOT:PSS interface could be enhanced by the introduction of impurity energy levels through doping. Thus, high-energy electrons absorbing mechanical energy generated by sliding or contact-separation motion are prone to be excited from PEDOT:PSS surface states to LUMO and then tunnel to the Al side. Besides, the improved transport properties of the PEDOT:PSS are also helpful for the carrier transport and the lowered device internal impedance. We then performed subsequent tests employing doped PEDOT:PSS film (ω_{DMSO} of 8%) as the optimized device.

2.4. Humidity-resistance, durability and applications

The output performance of typical triboelectric nanogenerators often decays significantly in high-humidity environment due to the leakage of electrostatic charges. Noteworthily, the TVNG exhibits an exceptional stability in high-humidity environment. The stability test was conducted in a glove box where the relative humidity (RH) of the environment can be controlled. The electrical outputs of the TVNG were recorded under varying humidity conditions. Interestingly, the current, voltage and transferred charge of TVNG in contact-separation mode and sliding mode remained stable when the RH is increased from 10% to 80%. Only very slight decrease in outputs was observed when RH reaches 90%, confirming excellent humidity resistance of the TVNG (Fig. 4a, b and Figure S14). In a high-humidity environment, a small broad peak of around 65 μA appears in contact-separation mode (right inset in Fig. 4a); while, in the sliding mode, the output current signal drops back to stay at approximately 153 μA instead of zero during the interval of each sliding (right inset of Fig. 4b). Although the *IV* curves of the Al/doped PEDOT:PSS film were slightly varied in different humidity conditions, the calculated Schottky barrier height slightly changes (Figure S15), proving that the tribovoltaic electrical signal is less affected by humidity variation (Fig. 4c). In high-humidity environment, the relaxation phenomenon of the electrical signal is likely to correspond to the electrochemical effect at the interfaces of Al and PSS. As moisture enters PSS (i.e., poly(4-styrenesulfonic acid)), the hydrogen ions in PSS are easily dissociated by water molecular. Ion transport becomes easier in high humidity environments as verified from the impedance of PEDOT:PSS films doped with 8% DMSO at various humidity in the frequency range from 0.1 to 10^6 Hz (Figure S16). To validate this effect, an Al foil block maintained continuous contact with pure PSS membrane cast on nickel at 90% relative humidity, resulting in stable electrical output of 0.4 V voltage and 54 μA current (Figure S17, S18), confirming the electrochemical effect as illustrated in Fig. 4d. Thus, the existence of a coupling effect of tribovoltaic (dominant) and electrochemical effect in this system is confirmed at high humidity (Fig. 4d).

Notably, the generator exhibits remarkable durability in contact-separation mode, with the current demonstrating no discernible degradation even after 100,000 motion cycles (Fig. 5a). Similarly, no noticeable deterioration in electrical outputs is observed after subjecting the PEDOT film to 36,000 cycles of bending at a 0.5 cm radius of curvature by a linear motor (Fig. 5b). With the input energy from three TVNGs in series connection, various capacitors can be instantaneously charged to 2.0 V (Figure S19). The 4.7 μF capacitor was charged to 2.57 V in 20 s and was immediately connected to a commercial watch, which worked continuously for more than 40 min driven by continuous reciprocating sliding motion (Fig. 5c), demonstrating a self-powered electronic device. Exceptional electrical outputs were achieved with current density of 27.85 A/m^{-2} and a peak power density of 9.16 W m^{-2} in contact-separation mode, and a J of 4.97 A/m^{-2}, an average charge density of 225.73 mC m^{-2} in sliding mode, surpassing most currently reported semiconductor direct current generators in various mechanical motions (Fig. 5d). A summary of the output performance, durability, and humidity sensitivity of this organic semiconductor generator and triboelectric nanogenerators is presented in Fig. 5e. The output voltage of triboelectric nanogenerators can reach several thousand volts, but, the current density, transferred charge density, and moisture resistance of the organic semiconductor generator surpass those of conventional triboelectric nanogenerators. This optimization method provides valuable guidance for high-performance TVNG devices and demonstrates great potential of which for further practical applications in distributed power.

3. Conclusion

In summary, we have demonstrated the improved electrical outputs and enhanced robustness of polymeric tribovoltaic nanogenerator through the secondary doping. With an optimum DMSO doping content of 8% in conjugated polymer PEDOT:PSS, the TVNG has achieved exceptional electrical outputs: a charge density of 150.48 mC m^{-2} and a peak power density of 9.16 W m^{-2} in contact-separation mode; superior charge density of 225.73 mC m^{-2} in sliding mode. The enhanced electrical outputs are attributed to the improved electrical properties of the polymer semiconductor and the optimized metal–semiconductor junction characteristics. Furthermore, the secondary doping also improved

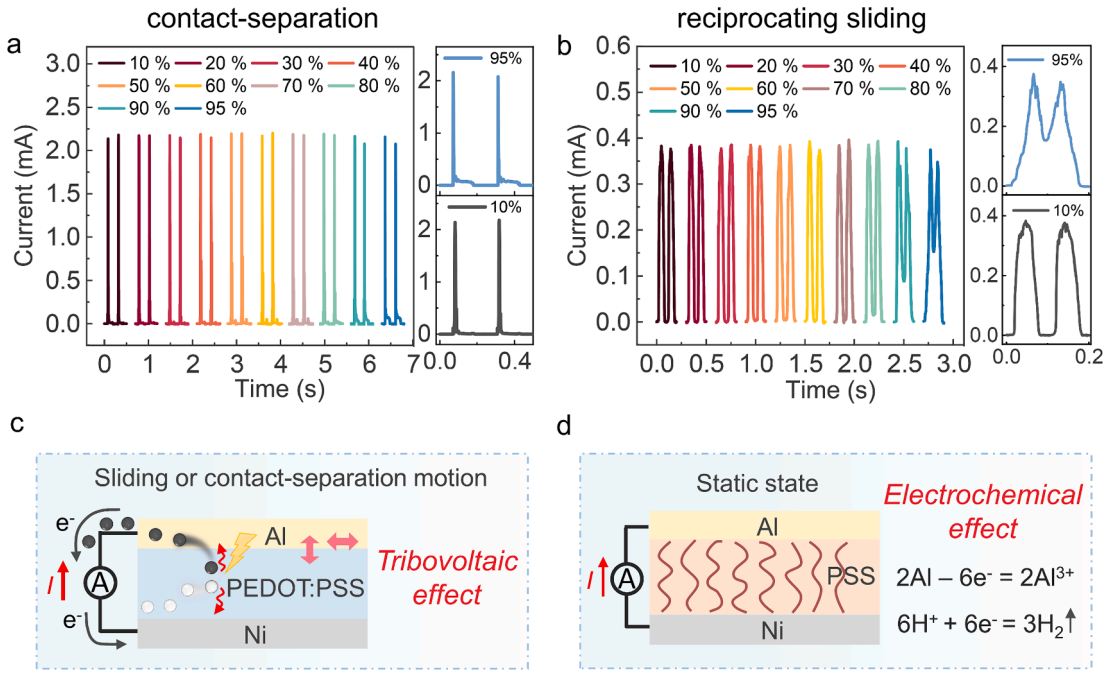

Fig. 4. Influence of humidity on the tribovoltaic outputs. Current outputs of the TVNG in (a) contact-separation and (b) sliding mode under different humidity. Schematic diagram of the (c) tribovoltaic effect and (d) electrochemical effect at high humidity condition.

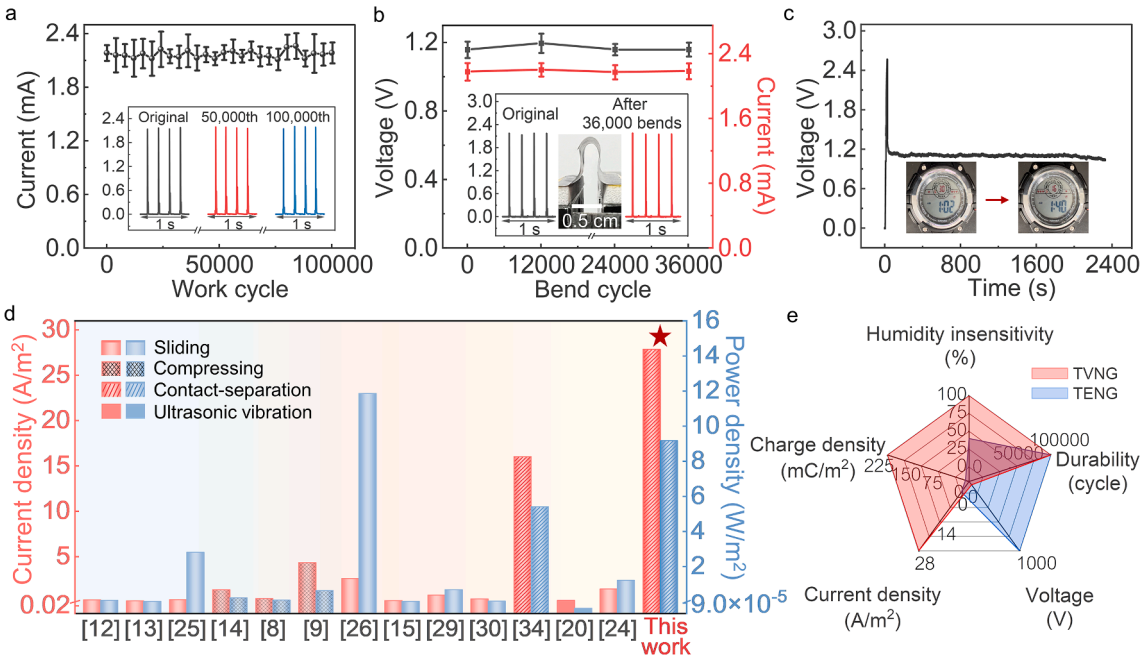

Fig. 5. Durability and application demonstration of the TVNG. (a) The current durability of the generator under the long-term contact-separation operation for 100,000 cycles. (b) The output after bending 36,000 times at a 0.5 cm curvature in contact-separation mode. (c) A commercial digital watch is constantly powered by the TVNG in sliding modes. (d) Comparison of power density and current density of the tribovoltaic nanogenerator with representative reports in the literature [8,9,12–15,20,24–26,29,30,34]. (e) Comparison of various properties between our flexible TVNG and triboelectric nanogenerators (TENG).

the flexibility of the PEDOT:PSS, and hence the mechanical robustness of TVNG. The device can withstand 100,000 contact-separation cycles or 36,000 bending cycles without degradation. Lastly, exceptional humidity resistance of the device has been confirmed, and the coupling of tribovoltaic and electrochemical effects in high-humidity conditions have been demonstrated.

4. Experimental

4.1. Materials

PEDOT:PSS, Poly(3,4-ethylenedioxythiophene)-poly(styrenesulfonate) (Solid content 1.3%, Heraeus), DMSO, Dimethyl sulfoxide (99%, Aladdin) were employed. All reagents were used as received without additional purification. High-purity aluminum films, nickel tapes,

solvent bottles and custom polytetrafluoroethylene molds were purchased online.

4.2. Fabrication of PEDOT:PSS films secondarily doped with DMSO

In Figure S1, 2 g of PH1000 solution were weighed and placed into seven pre-marked 10 mL glass solvent bottles, respectively. Subsequently, 1 g of deionized water was added to each bottle, and DMSO solutions with different weight percentages were added (ω of 0%, 2%, 5%, 8%, 10%, and 15%), respectively. The mixture solution was stirred for a duration of 2 h, employing an 80 °C heated stirring table. The solution was then transferred into custom-made seven polytetrafluoroethylene molds. Afterward, the solution was allowed to stand for 10 min, enabling the removal of air bubbles that may have formed during the stirring process. Then, the molds filled with the solution were positioned in a dry box. Over a period of 12 h, the solution underwent evaporation at 35 °C, resulting in the simultaneous removal of water and a portion of the solvent, leading to the formation of an initial thin film. Subsequently, the films were subjected to an annealing process at 150 °C for a duration of 1 h, which facilitated recrystallization via solvent evaporation. Finally, the films were exposed to a temperature of 60 °C for 12 h, ensuring the near-complete removal of any residual solvent.

4.3. Characterizations and experiment setup

The scanning electron microscope (SEM) images of PEDOT:PSS films doped with DMSO were characterized by a FEI Nova Nano SEM 450. X-ray diffraction pattern of PEDOT:PSS samples were measured by XRD powder (Xpert3 Powder). The FTIR spectrum were measured with Fourier transform infrared spectrometer (VERTEX80v). Raman spectrum were measured by Confocal Micro Raman Spectrometer (Lab RAM HR Evolution). The conductivity, mobility, and carrier concentration of the doped films were measured by an Efficient Hall test (High Resistance HALL). Ultraviolet Photoelectron Spectroscopy (UPS) was performed by PHI 5000 Versa Probe III (Scanning ESCA Microprobe) with He I source (21.22 eV). UV Vis Near-Infrared Diffuse Reflectance spectrum were measured by Shimadzu UV-3600i Plus. The current and voltage output were measured with a Keithley 6514/6517 Electrometer. The elongation at break, tensile strength and corresponding Young's modulus of the films were measured by a universal testing machine (YL-S71). The electrochemical impedance spectroscopy of the films was measured by an electrochemical workstation (CHI 760E). The force on the generator were measured by a digital Force Gauge (ZTA-DPU-11). The current–voltage test of the Al/PEDOT:PSS interface were measured by Keithley 2450 Source Meter.

CRediT authorship contribution statement

Jia Meng: Writing – review & editing, Writing – original draft, Visualization, Validation, Software, Resources, Project administration, Methodology, Investigation, Formal analysis, Data curation, Conceptualization. **Chuntao Lan:** Writing – review & editing, Supervision, Funding acquisition. **Chongxiang Pan:** Visualization, Validation, Supervision, Project administration. **Jun Yang:** Supervision, Project administration. **Xiong Pu:** Writing – review & editing, Supervision, Funding acquisition. **Zhong Lin Wang:** Writing – review & editing, Supervision, Funding acquisition.

Declaration of competing interest

The authors declare that they have no known competing financial interests or personal relationships that could have appeared to influence the work reported in this paper.

Data availability

Data will be made available on request.

Acknowledgements

The authors thank for the support from the National Key R & D Project from the Minister of Science and Technology (2021YFA1201603), the National Natural Science Foundation of China (52173274), the grants from Chinese Academy of Sciences (124GJHZ2023031MI), and the Fundamental Research Funds for the Central Universities.

Appendix A. Supplementary data

Supplementary data to this article can be found online at https://doi.org/10.1016/j.cej.2024.150412.

References

[1] M.L. Zhu, Z.D. Sun, Z.X. Zhang, Q.F. Shi, T.Y.Y. He, H.C. Liu, T. Chen, C.K. Lee, Haptic-feedback smart glove as a creative human-machine interface (HMI) for virtual/augmented reality applications, Sci. Adv. 6 (19) (2020) eaaz8693, https://doi.org/10.1126/sciadv.aaz8693.
[2] W.H. Xu, H.X. Zheng, Y. Liu, X.F. Zhou, C. Zhang, Y.X. Song, X. Deng, M. Leung, Z. B. Yang, R.X. Xu, Z.L. Wang, X.C. Zeng, Z.K. Wang, A droplet-based electricity generator with high instantaneous power density, Nature 578 (7795) (2020) 392–396, https://doi.org/10.1038/s41586-020-1985-6.
[3] R.Y. Liu, Z.L. Wang, K. Fukuda, T. Someya, Flexible self-charging power sources, Nat. Rev. Mater. 7 (11) (2022) 870–886, https://doi.org/10.1038/s41578-022-00441-0.
[4] T. Wang, Y. Zhang, W.Y. Kong, L. Qiao, B.G. Peng, Z.C. Shen, Q.F. Han, H. Chen, Z. L. Yuan, R.K. Zheng, X.D. Yang, Transporting holes stably under iodide invasion in efficient perovskite solar cells, Science 377 (6611) (2022) 1227–1231, https://doi.org/10.1126/science.abq6235.
[5] A. Chen, Q.X. Zeng, L.M. Tan, F. Xu, T.Y. Wang, X.F. Zhang, Y.L. Luo, X. Wang, A novel hybrid triboelectric nanogenerator based on the mutual boosting effect of electrostatic induction and electrostatic breakdown, Energy Environ. Sci. 16 (8) (2023) 3486–3496, https://doi.org/10.1039/d3ee01658g.
[6] Z.L. Wang, J.H. Song, Piezoelectric nanogenerators based on zinc oxide nanowire arrays, Science 312 (5771) (2006) 242–246, https://doi.org/10.1126/science.1124005.
[7] C.C. Shan, K.X. Li, Y.T. Cheng, C.G. Hu, Harvesting environment mechanical energy by direct current Triboelectric nanogenerators, Nano-Micro Lett. 15 (1) (2023) 127, https://doi.org/10.1007/s40820-023-01115-4.
[8] H. Shao, J. Fang, H. Wang, H. Zhou, H. Niu, F. Chen, G. Yan, S. Fu, Y. Cao, T. Lin, Doping effect on conducting Polymer-metal schottky DC generators, Adv. Electron. Mater. 5 (2) (2018) 1800675, https://doi.org/10.1002/aelm.201800675.
[9] X. Ding, H. Shao, H.X. Wang, W.D. Yang, J. Fang, D.Q. Zhang, T. Lin, Schottky DC generators with considerable enhanced power output and energy conversion efficiency based on polypyrrole-TiO_2 nanocomposite, Nano Energy 89 (2021) 106367, https://doi.org/10.1016/j.nanoen.2021.106367.
[10] Z.L. Wang, A.C. Wang, On the origin of contact-electrification, Mater. Today 30 (2019) 34–51, https://doi.org/10.1016/j.mattod.2019.05.016.
[11] M.L. Zheng, S.Q. Lin, L. Xu, L.P. Zhu, Z.L. Wang, Scanning probing of the tribovoltaic effect at the sliding Interface of two semiconductors, Adv. Mater. 32 (21) (2020) e2000928.
[12] U. Liu, M.I. Cheikh, R.M. Bao, H.H. Peng, F.F. Liu, Z. Li, K.R. Jiang, J. Chen, T. Thundat, Tribo-tunneling DC generator with carbon aerogel/silicon multi-nanocontacts, Adv. Electron. Mater. 5 (12) (2019) 1900464, https://doi.org/10.1002/aelm.201900464.
[13] Z. Zhang, D. Jiang, J. Zhao, G. Liu, T. Bu, C. Zhang, Z.L. Wang, Tribovoltaic effect on metal-semiconductor interface for direct-current low-impedance triboelectric nanogenerators, Adv. Energy Mater. 10 (9) (2020) 1903713, https://doi.org/10.1002/aenm.201903713.
[14] H. Shao, J. Fang, H.X. Wang, H.T. Niu, H. Zhou, Y.Y. Cao, F.Y. Chen, S.D. Fu, T. Lin, Schottky direct-current energy harvesters with large current output density, Nano Energy 62 (2019) 171–180, https://doi.org/10.1016/j.nanoen.2019.05.037.
[15] J. Meng, Z.H. Guo, C.X. Pan, L.Y. Wang, C.Y. Chang, L.W. Li, X. Pu, Z.L. Wang, Flexible textile direct-current generator based on the tribovoltaic effect at dynamic metal-semiconducting polymer interfaces, Acs Energy Lett. 6 (7) (2021) 2442–2450, https://doi.org/10.1021/acsenergylett.1c00288.
[16] R. Xu, Q. Zhang, J.Y. Wang, D. Liu, J. Wang, Z.L. Wang, Direct current triboelectric cell by sliding an n-type semiconductor on a p-type semiconductor, Nano Energy 66 (2019) 104185, https://doi.org/10.1016/j.nanoen.2019.104185.
[17] R.Z. Yang, Z.H. He, S.Q. Lin, W.J. Dou, Z.L. Wang, H.Y. Wang, J. Liu, Tunable tribovoltaic effect via metal-insulator transition, Nano Lett. 22 (22) (2022) 9084–9091, https://doi.org/10.1021/acs.nanolett.2c03481.
[18] J. Tan, S.M. Fang, Z.H. Zhang, J. Yin, L.X. Li, X. Wang, W.L. Guo, Self-sustained electricity generator driven by the compatible integration of ambient moisture

adsorption and evaporation, Nat. Comm. 13 (1) (2022) 3643, https://doi.org/10.1038/s41467-022-31221-7.
[19] H. Jin, S.G. Yoon, W.H. Lee, Y.H. Cho, J. Han, J. Park, Y.S. Kim, Identification of water-infiltration-induced electrical energy generation by ionovoltaic effect in porous CuO nanowire films, Energy & Environ. Sci. 13 (10) (2020) 3432–3438, https://doi.org/10.1039/d0ee02190c.
[20] W.B. Seh, R. Xu, S. Deng, Z. Sun, Z. Wang, Z. Fan, L. Wei, Q. Zhang, Harvesting and mapping ultrasonic vibration power using semiconducting wire-based tribovoltaic generators, Nano Energy 116 (2023) 108837, https://doi.org/10.1016/j.nanoen.2023.108837.
[21] Y. Yan, X. Zhou, S. Feng, Y. Lu, J. Qian, P. Zhang, X. Yu, Y. Zheng, F. Wang, K. Liu, S. Lin, Direct current electricity generation from dynamic polarized water-semiconductor interface, J. Phys. Chem. C 125 (26) (2021) 14180–14187, https://doi.org/10.1021/acs.jpcc.1c02078.
[22] Y.-S. Lee, S. Jeon, D. Kim, D.-M. Lee, D. Kim, S.-W. Kim, High performance direct current-generating triboelectric nanogenerators based on tribovoltaic p-n junction with ChCl-passivated CsFAMA perovskite, Nano Energy 106 (2023) 108066, https://doi.org/10.1016/j.nanoen.2022.108066.
[23] Y.H. Lu, Q.Y. Gao, X.T. Yu, H.N. Zheng, R.J. Shen, Z.Z. Hao, Y.F. Yan, P.P. Zhang, Y. Wen, G.T. Yang, S.S. Lin, Interfacial built-in electric field-driven direct current generator based on dynamic silicon homojunction, Research 2020 (2020) 5714754, https://doi.org/10.34133/2020/5714754.
[24] F. Jiang, G. Thangavel, X. Zhou, G. Adit, H. Fu, J. Lv, L. Zhan, Y. Zhang, P.S. Lee, Ferroelectric modulation in flexible Lead-free perovskite schottky direct-current nanogenerator for capsule-like magnetic suspension sensor, Adv. Mater. 35 (31) (2023) 2302815, https://doi.org/10.1002/adma.202302815.
[25] Z.Z. Wang, Z. Zhang, Y.K. Chen, L.K. Gong, S.C. Dong, H. Zhou, Y. Lin, Y. Lv, G. X. Liu, C. Zhang, Achieving an ultrahigh direct-current voltage of 130 V by semiconductor heterojunction power generation based on the tribovoltaic effect, Energy & Environ. Sci. 15 (6) (2022) 2366–2373, https://doi.org/10.1039/d2ee00180b.
[26] Z. Zhang, Z.Z. Wang, Y.K. Chen, Y. Feng, S.C. Dong, H. Zhou, Z.L. Wang, C. Zhang, Semiconductor contact-electrification-dominated tribovoltaic effect for ultrahigh power generation, Adv. Mater. 34 (20) (2022) 2200146, https://doi.org/10.1002/adma.202200146.
[27] X. Huang, X. Xiang, J. Nie, D. Peng, F. Yang, Z. Wu, H. Jiang, Z. Xu, Q. Zheng, Microscale schottky superlubric generator with high direct-current density and ultralong life, Nat. Comm. 12 (1) (2021) 2268, https://doi.org/10.1038/s41467-021-22371-1.
[28] L.Q. Zhang, H.F. Cai, L. Xu, L. Ji, D.A. Wang, Y.B. Zheng, Y.G. Feng, X.D. Sui, Y. F. Guo, W.L. Guo, F. Zhou, W.M. Liu, Z.L. Wang, Macro-superlubric triboelectric nanogenerator based on tribovoltaic effect, Matter 5 (5) (2022) 1532–1546, https://doi.org/10.1016/j.matt.2022.02.021.
[29] R.Z. Yang, M. Benner, Z.P. Guo, C. Zhou, J. Liu, High-performance flexible schottky DC generator via metal/conducting polymer sliding contacts, Adv. Funct. Mater. 31 (43) (2021) 2103132, https://doi.org/10.1002/adfm.202103132.
[30] Z. You, S. Wang, Z. Li, Y. Zou, T. Lu, F. Wang, B. Hu, X. Wang, L. Li, W. Fang, Y. Liu, High current output direct-current triboelectric nanogenerator based on organic semiconductor heterojunction, Nano Energy 91 (2022) 106667, https://doi.org/10.1016/j.nanoen.2021.106667.
[31] X. Yin, B.G. Xu, C.W. Kan, Y.J. Yang, Dynamic perovskite homojunction based light-assisted, direct current tribovoltaic nanogenerators, Adv. Energy Mater. 13 (2023) 2301289, https://doi.org/10.1002/aenm.202301289.
[32] W.Y. Qiao, L.L. Zhou, Z.H. Zhao, P.Y. Yang, D. Liu, X.R. Liu, J.Q. Liu, D.Y. Liu, Z. L. Wang, J. Wang, MXene lubricated tribovoltaic nanogenerator with high current output and long lifetime, Nano-Micro Lett. 15 (1) (2023) 218, https://doi.org/10.1007/s40820-023-01198-z.
[33] H. Yuan, Z. Xiao, J. Wan, Y. Xiang, G. Dai, H. Li, J. Yang, A rolling-mode Al/CsPbBr 3 schottky junction direct-current triboelectric nanogenerator for harvesting mechanical and solar energy, Adv. Energy Mater. 12 (25) (2022) 2200550, https://doi.org/10.1002/aenm.202200550.
[34] J. Meng, C.X. Pan, L.W. Li, Z.H. Guo, F. Xu, L.Y. Jia, Z.L. Wang, X. Pu, Durable flexible direct current generation through the tribovoltaic effect in contact-separation mode, Energy & Environ. Sci. 15 (12) (2022) 5159–5167, https://doi.org/10.1039/d2ee02762c.
[35] T. Horii, Y.C. Li, Y. Mori, H. Okuzaki, Correlation between the hierarchical structure and electrical conductivity of PEDOT/PSS, Polym. J. 47 (10) (2015) 695–699, https://doi.org/10.1038/pj.2015.48.
[36] E. Hosseini, V. Ozhukil Kollath, K. Karan, The key mechanism of conductivity in PEDOT:PSS thin films exposed by anomalous conduction behaviour upon solvent-doping and sulfuric acid post-treatment, J. Mater. Chem. C 8(12) (2020) 3982-3990, doi: 10.1039/c9tc06311k.
[37] N. Kim, S. Kee, S.H. Lee, B.H. Lee, Y.H. Kahng, Y.R. Jo, B.J. Kim, K. Lee, Highly conductive PEDOT:PSS nanofibrils induced by solution-processed crystallization, Adv. Mater. 26 (14) (2013) 2268–2272, https://doi.org/10.1002/adma.201304611.
[38] N. Kim, B.H. Lee, D. Choi, G. Kim, H. Kim, J.R. Kim, J. Lee, Y.H. Kahng, K. Lee, Role of interchain coupling in the metallic state of conducting polymers, Phys. Rev. Lett. 109 (10) (2012) 106405, https://doi.org/10.1103/PhysRevLett.109.106405.
[39] S. Lee, K.K. Gleason, Enhanced optical property with tunable band gap of cross-linked PEDOT Copolymers via oxidative chemical vapor deposition, Adv. Funct. Mater. 25 (1) (2014) 85–93, https://doi.org/10.1002/adfm.201402924.
[40] F. Yan, E.P.J. Parrott, B.S.Y. Ung, E. Pickwell-MacPherson, Solvent doping of PEDOT/PSS: effect on terahertz optoelectronic properties and utilization in terahertz Devices, J. Phys. Chem. C 119 (12) (2015) 6813–6818, https://doi.org/10.1021/acs.jpcc.5b00465.
[41] Y.J. Lin, J.Y. Lee, S.M. Chen, Changing electrical properties of PEDOT:PSS by incorporating with dimethyl sulfoxide, Chem. Phys. Lett. 664 (2016) 213–218, https://doi.org/10.1016/j.cplett.2016.10.038.
[42] W.-S.N. Yow-Jon Lin, Jhe-You Lee Effect of incorporation of ethylene glycol into PEDOT:PSS on electron phonon coupling and conductivity, J. Appl. Phys. 117 (2015) 215501, doi: 10.1063/1.4921930.
[43] Y. Wang, C.X. Zhu, R. Pfattner, H.P. Yan, L.H. Jin, S.C. Chen, F. Molina-Lopez, F. Lissel, J. Liu, N.I. Rabiah, Z. Chen, J.W. Chung, C. Linder, M.F. Toney, B. Murmann, Z. Bao, A highly stretchable, transparent, and conductive polymer, Sci. Adv. 3 (3) (2017), https://doi.org/10.1126/sciadv.1602076.